Quench experiments on sub-size HTS Cable-In-Conduit Conductors for fusion applications: Data analysis and model validation

Cryogenics 132 (2023) 103695

Contents lists available at ScienceDirect

Cryogenics

journal homepage: www.elsevier.com/locate/cryogenics

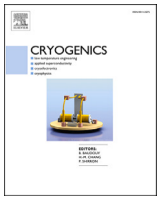

Research paper

Quench experiments on sub-size HTS Cable-In-Conduit Conductors for fusion applications: Data analysis and model validation

A. Zappatore [a,*], R. Bonifetto [a], P. Bruzzone [b], V. Corato [c], O. Dicuonzo [d], M. Kumar [d], K. Sedlak [b], B. Stepanov [e]

[a] NEMO group, Dipartimento Energia, Politecnico di Torino, Torino, Italy
[b] Ecole Polytechnique Fédérale de Lausanne (EPFL), Swiss Plasma Center (SPC), CH-5232 Villigen PSI, Switzerland
[c] Superconductivity Section, ENEA, Frascati, Italy
[d] Former at Ecole Polytechnique Fédérale de Lausanne (EPFL), Swiss Plasma Center (SPC), CH-5232 Villigen PSI, Switzerland
[e] Retired from Ecole Polytechnique Fédérale de Lausanne (EPFL), Swiss Plasma Center (SPC), CH-5232 Villigen PSI, Switzerland

ARTICLE INFO

Keywords:
HTS
Quench
Experiments
Modeling
Validation

ABSTRACT

The recent experimental campaign, carried out in the upgraded SULTAN facility and supported by EUROfusion, investigated quench propagation in high field, sub-size HTS Cable-In-Conduit Conductors. The available experimental data consist of voltage, jacket and helium temperatures measured along the length of the conductors. In this work, the analysis of experimental data is carried out, focusing on the normal zone propagation velocity and the hotspot temperature reached during the quench. The validation of one-dimensional (1D) thermal-hydraulic and electric numerical models implemented in the H4C code is presented, showing very good agreement between experimental and computed results, both in terms of global and local quantities. The validated tool is then used to assess the impact on the hotspot measured in SULTAN and that reached in a uniform magnetic field configuration, showing that SULTAN measurements provide conservative assessments. The tool is then used to simulate a quench in a real-case scenario, i.e., the EU DEMO Central Solenoid operation, showing that a conventional quench detection strategy based on voltage measurements should suffice, leading to hotspot temperature around 250 K.

1. Introduction

The magnet system of the EU DEMO tokamak is under its conceptual design phase within the EUROfusion Consortium [1]. The Central Solenoid (CS) will be made of five modules. Two options are currently under investigation for the design of the CS modules. One is based on an ITER-like pancake-wound coil made of Nb_3Sn Cable-In-Conduit Conductors (CICCs). The other option is based on a hybrid layer-wound coil, made of High Temperature Superconducting (HTS) CICCs for the innermost layers (high field) and Low Temperature Superconducting CICCs for the outermost ones (middle-low field) [2]. The first solution would be more conservative, as it is based on a mature technology already used to build similar coils for large-scale machines, e.g. ITER [3] and JT-60SA [4]. The second option is less technologically mature, but it would be more cost-effective, enhancing the performance of the machine [5]. Furthermore, the research and development on HTS conductors for fusion magnets is continuously growing, as shown by the recent achievements of different projects worldwide, see the reviews [6] and [7]. Several conductor designs are relying on the CICC concept, such as those proposed by ENEA [8], Swiss Plasma Center [9], Karlsruhe Institute of Technology [10], Advanced Conductor Technology [11], Commonwealth Fusion Systems [12], North China Electric Power University [13].

One of the peculiarities of HTS conductors with respect to Low Temperature Superconducting (LTS) ones is the different behavior during quench propagation. It is well known that the Normal Zone Propagation Velocity (NZPV) in HTS tapes is much smaller than in LTS [14], thus leading to a delayed quench detection, if based on voltage, in turn meaning a possibly more dangerous coil operation. Therefore, EUROfusion has launched an experimental campaign to investigate the quench propagation in high field, sub-size CICCs made of HTS, for which available data are currently lacking. The quench tests should also serve as

* Corresponding author.
E-mail address: andrea.zappatore@polito.it (A. Zappatore).

https://doi.org/10.1016/j.cryogenics.2023.103695
Received 3 November 2022; Received in revised form 19 May 2023; Accepted 24 May 2023
Available online 29 May 2023

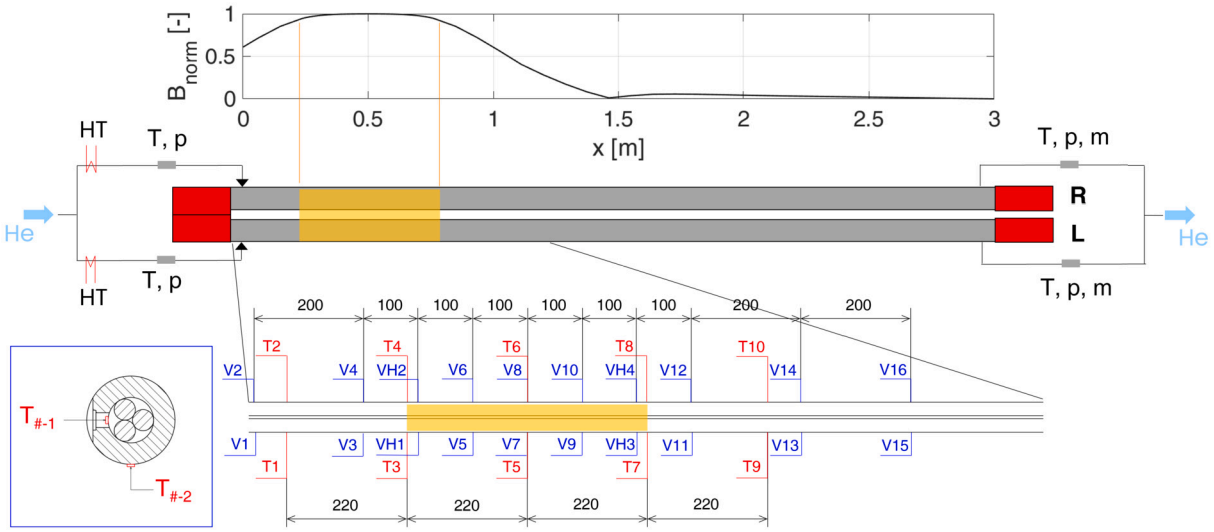

Fig. 1. Sketch of the conductor diagnostics: in the center, the two conductors (R = right, L = left) are shown with the inlet and outlet sensors (T = temperature, p = pressure, m = mass flow) and heaters (HT). The bottom (on the left in the figure) and top (on the right in the figure) terminations are represented in red. In the top, normalized magnetic field distribution along the conductors. In the bottom, detailed view of the voltage taps and temperature sensors placed along the conductors. In the blue box, cut view of the conductor, showing that each temperature sensor location, jacket (T#-2) and helium (T#-1) temperatures are measured. The High Field Zone is highlighted in yellow. x = 0 is in correspondence of the helium inlet. (For interpretation of the colors in the figure(s), the reader is referred to the web version of this article.)

an opportunity to validate numerical models which are typically used for the study of this phenomenon, such as the 4C code [15] or THEA [16]. Several numerical studies of quench propagation in HTS conductors for fusion have been carried out, see e.g., [17], [18], but none of the models used therein was validated due to the lack of experimental data. However, code validation, i.e., the comparison of the computed results with experimental data, is a key step in the assessment of the reliability of a numerical tool [19].

The aim of the work presented here is the analysis of the data collected on the conductors, the validation of a numerical tool and the simulation of the quench evolution in a DEMO-relevant condition, using the tool validated on the available measurements of the sub-sized conductor.

The numerical tool adopted to model the quench propagation is the H4C code [20], recently developed at Politecnico di Torino, which is devoted to the simulation of fast electric and/or thermal-hydraulic transients in HTS conductors.

The work is organized as follows: first the experimental setup is briefly described and the experimental data are analyzed, with a focus on the normal zone propagation velocity and hotspot temperature. Then, the numerical model development is briefly described and the comparison of the experimental data with the computed ones is discussed. In the last section, the application of the validated tool to a real-case scenario, e.g., that foreseen for the EU DEMO CS, is presented.

2. Experimental setup

The tests have been performed in SULTAN. The facility was recently upgraded and it can now provide a maximum current of 15 kA at 2 V [21]. The SULTAN sample is made of two conductors which are electrically connected in series through the bottom joint. The helium is provided separately to each conductor, meaning that each conductor can be tested separately. The He inlets are placed after the joints, thus their influence on the He flow is automatically excluded. The conductor length is 3.6 m long and the magnetic field has a uniform length of about 44 cm, called High Field Zone (HFZ) as shown in Fig. 1. The arrangement of the voltage taps and temperature sensors is also shown in Fig. 1. The conductors were equipped with voltage taps along the conductor axis and placed on the conductor jacket. Temperature sensors were used to measure the temperature of the steel jacket and of the helium in the same cross section. The jacket temperature sensors are attached to the outside wall, while the helium ones are intrusive in the conductor [21]. All the conductors tested differ from the others for a single major feature. The cross section of the jacket, that of copper and that available to the helium were kept equal for all the conductors. Here we focus the analyzes on two conductors, namely the *reference* and the *non-twisted* conductors. They are made of 3 strands, each of which is made of a stack of REBCO tapes enclosed in a copper profile (total copper cross-section, including the tape stabilizer, A_{Cu} = 150 mm^2) and they are equal, except for the twisting of the cable and of the HTS stack in the strands, see [21] for further details on the conductor design. This major difference implies also a difference in the n-value of the conductor, see Section 3.1.1 and possibly in the thermal contact resistance between strands and jacket. In the reference conductor, each strand is twisted with a twist pitch equal to 400 mm, then the strand triplet is twisted with a twist pitch equal to 1000 mm.

The test program included DC performance tests to measure the critical current I_C and the current sharing temperature T_{CS} and quench tests in different conditions of magnetic field and current. The quench was always initiated by heating the helium upstream the inlet of the conductors, using electric heaters, see Fig. 1. Fast, i.e., few seconds long, constant heat pulse, or slow, i.e., increasing and up to few minutes long until quench is induced, heating of the helium were tested in order to assess the impact of the heating mode on the quench propagation. The time-delay for the initiation of the current dump is based on the temperature and electric field thresholds, which were different for each shot, in order to let the quench propagate more or less. This is further explained in the section 3.2. The list of the quench shots analyzed in this work, together with their key features are reported in Table 1. The mass flow rate in all the shots reported in Table 1 is equal to 1.5 g/s. Note that the fast heating for the non-twisted conductor required a shorter time to quench the conductor than for the reference one because of less stability, as discussed in section 3.2.1. In all the fast heating shot, the heater was charged at its maximum power (80 W).

3. Experimental results

In this section, the DC performance of the conductors, which are essential to prepare the input of the numerical model, as well as the quench results, are analyzed and discussed.

Table 1
Quench shots with their key parameters.

Shot #	Current (kA)	Magnetic field (T)	Heating mode	Heating duration (s)
Non-twisted conductor				
170802	15	6	Fast	15
170803	15	6	Fast	15
170804	15	6	Fast	15
170805	15	6	Fast	15
170806	15	6	Fast	15
170808	15	6	Fast	15
190804	15	6	Fast	15
190808	15	6	Slow	–
190805	11*	10	Fast	15
200802	11*	10	Slow	–
Reference conductor				
101102	15	3.5	Fast	65
101103	15	3.5	Fast	65
101104	15	3.5	Fast	65
161101	15	3.5	Fast	65
161102	15	3.5	Fast	65
161103	15	3.5	Slow	–
161104	15	3.5	Slow	–
161106	15	3.5	Slow	–
181101	9.5*	9	Slow	–

*Low current shots (all the others are those at high current).

3.1. DC performance

3.1.1. Critical current

The cable critical current is extracted fitting the average electric field measured with the voltage taps "VH" in the HFZ, see Fig. 1, as function of the applied current with the power law reported in Equation (1),

$$E = E_{offset} + E_C \left(\frac{I}{I_C} \right)^n \tag{1}$$

where E_{offset} is an electric field offset, E_C is the critical field equal to 100 μV/m, I is the transport current, I_C is the critical current, n is the n-value of the cable, which rules the transition from the superconducting to the normal state. The voltage, thus the electric field, is averaged in each time interval when the current is constant.

The critical current is then used to compute the "effective" superconducting cross-section which is then used as input for the numerical model. The calculation is simply done according to Equation (2),

$$A_{SC} = \frac{I_C}{J_C(B,T)} \tag{2}$$

where A_{SC} is the cable (total) superconducting cross-section and J_C is the superconductor scaling law taken from [22], B is the magnetic field and T the superconductor temperature. Below 10 K, the helium and jacket temperature are practically the same. The values of critical current and n-value are reported in Table 2.

3.1.2. Current sharing temperature

The current sharing temperature is taken as the value at which the electric field in the HFZ reaches $E_C = 100$ μV/m. Also in this case, the VH sensors across the HFZ are considered.

When available, tests at different magnetic fields have been analyzed. This allowed a cross-check of the soundness of the scaling law adopted for the modeling of the samples. The values of T_{CS} measured with 15 kA are reported in Table 2.

3.2. Quench experiments

In this section, the analysis of the experimental results is carried out. Key features of the quench propagation, such as the NZPV and the hotspot temperature, are assessed.

Table 2
DC performance of the two conductors analyzed.

	Not-twisted	Reference
I_C (kA)	13.9 (7 K, 7 T)	14.5 (5.6 K, 4 T)
T_{CS} (K)	7.17 (15 kA, 6 T)	6.96 (15 kA, 3.5 T)
n-value	16.4	8.6

3.2.1. Normal zone propagation velocity

The NZPV is assessed considering the voltage measurements. The reason is that, in principle, the voltage signals are the most reliable for this estimation since they instantly react to the normal zone propagation. The alternative could be to use the temperature measurements. However, they typically react on the scale of seconds and such delays are not acceptable for the purpose of assessing the NZPV. The rationale followed for the estimation of the NZPV in the HFZ is the same adopted for the analysis of quench in LTS [23] and it is summarized below.

To fix the ideas, let us suppose that the quench starts in V5-V7, i.e., between voltage taps V5 and V7. Let us also focus on only one front, e.g., the downstream front, i.e., the front that is propagating towards the helium outlet. As soon as the front enters the region between V7-V9, the voltage measured by that couple of voltage taps starts increasing at time t_{V7V9}. The front travels and then enter the region between V9 and VH3. Here a resistive voltage starts to be measured, say at t_{V9VH3}. Therefore, the front took $\Delta t = t_{V9VH3} - t_{V7V9}$ to travel from V7 to V9, thus to travel $\Delta L = 10$ cm. The average velocity in that interval can then be computed as $NZPV = \Delta L/\Delta t$. From this, it is clear that to compute a single value of propagation speed, two couples of voltage taps are needed. It is also clear that the couple in which the resistive voltage is measured first, i.e. the portion in which the quench starts propagating, cannot be used to estimate the NZPV there.

The propagation of the upstream front, in case the quench starts in V5-V7, can be characterized with a single value of speed, i.e., that computed using VH1-V5 and V3-VH1. Instead, two values of NZPV can be computed for the downstream front using V7-V9 with V9-VH3 and V9-VH3 with VH3-V11. Note that the region of interest to quantify NZPV is the HFZ, thus V11-V13 and V1-V3 are not used for this purpose, since the sharp decrease of the magnetic field strongly impacts the NZPV.

Another crucial point is to define a voltage, or, equivalently, an average electric field, to confirm that the front has entered for the first time between a couple of voltage sensors. Here a threshold of $E_{threshold} = 1$ mV/cm will be used, see Fig. 2. This threshold has been set high enough to exclude sensors noise and voltage increase due to the warm helium, which in fact causes a knee in the voltage reading at values ≤ 0.1 mV/cm. Furthermore, at 1 mV/cm the critical current (at about 70 K, as derived in the next section) is ~100 A, thus ensuring that all the current is flowing in the copper, i.e. the superconductor is actually normal. A further increase of the $E_{threshold}$ has been verified not to lead to noticeable changes in the NZPV.

There are shots in which the electric field in V9-V7 crosses first the threshold, i.e., the quench is assumed to start propagating there, therefore the velocities that can be computed are those between V5-V7, VH1-V5 and V9-VH3. In any case, using this strategy, three values of NZPV can be computed, at best: two for the upstream front and one for the downstream front or vice-versa.

Results on selected shots for each type, i.e., fast/slow heating, high/low current, thus high/low copper current density J_{Cu}, are reported in Fig. 3. Starting from the non-twisted conductor, it can be seen that the quench is initiated either between V5-V7 or V7-V9 in case of fast heating and high J_{Cu}, see 170802 and 170804 in Fig. 3(a). Nevertheless, the NZPV retrieved is similar, regardless of the exact location where the quench starts propagating, i.e., 20-30 mm/s for the upstream front and 50-70 mm/s for the downstream front, see Table 3. This asymmetry hints the non-negligible role of the helium in facilitating the quench propagation downstream.

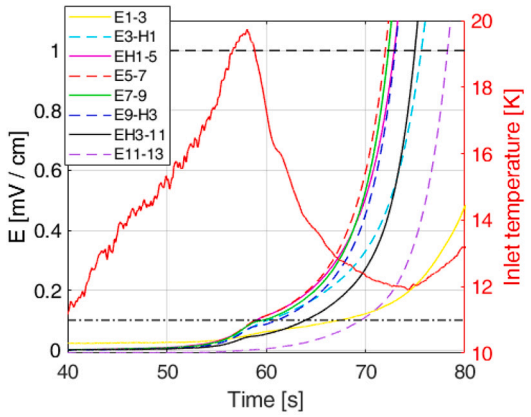

Fig. 2. Evolution of the average electric field and inlet temperature during shot 170802 (non-twisted conductor, 15 kA, 6 T, fast heating mode). The two reference values at 0.1 and 1 mV/cm are also shown.

Comparing the shots with high and low J_{Cu}, it is evident a smaller NZPV in case of lower J_{Cu}, see 190805 compared to 170804 or 200802 compared to 190808. This can be explained because, in the adiabatic case, the NZPV is found to be directly proportional to J_{Cu} [24]. Therefore, it is expected to have a slower quench propagation in case of lower J_{Cu}. Quantitatively, this corresponds to a variation from 20-40 mm/s (upstream front of 170804) to 6 mm/s (upstream front of 190805) and to a decrease from 26-55 mm/s (upstream front of 190808) to 15-30 mm/s (upstream front of 200802).

Concerning the heating speed, in case of a slow heating, the quench starts towards the end of the HFZ, because the warm helium is gradually heated also by the HFZ which is already in current sharing. This behavior is also discussed on the basis of the computed results in Section 5.5. In case of a fast heating, this effect is not visible because the helium temperature is more peaked and it tends to induce the quench at (or slightly after) the magnetic center.

The effect of the heating strategy is small in case of high J_{Cu}, because the propagation is mainly driven by the J_{Cu} itself, see shot 190808 compared to 170802 and 170804. On the other hand, in case of low J_{Cu}, a faster propagation is evident in case of slow heating, see shot 200802 compared to 190805. The faster propagation is due to a more uniform temperature of the HFZ; thus, as soon as the quench is initiated, it can propagate easier because of a reduced temperature margin with respect to the case with a fast heating.

Note that, according to the strategy reported above, the quench starts sometimes between V5-V7 and some other times between V7-V9. However, the electric field in V5-V7 and V7-V9 is always very close and where the quench starts depends on $E_{threshold}$. As a result, high values of NZPV can be found, while, on the other hand, VH1-V5 and V9-VH3, being always further from the initiation zone and closer to the end of the HFZ, lead to smaller NZPV. In any case, the strategy adopted and the data available lead to range of NZPV that is from 20 to 70 mm/s (neglecting the values found very close to the initiation region), confirming that the NZPV in HTS CICCs is 1-2 orders of magnitude lower than in LTS CICCs [23].

Concerning the reference conductor, the results in terms of quench front propagation for representative shots are reported in Fig. 3(b), while the detailed calculation of NZPV for all the analyzed shots is reported in Table 4. It can be seen that the repeatability of the results on the reference conductor is much better than the non-twisted ones, both in terms of quench initiation region and in terms of values of NZPVs (provided the heating mode is the same).

The impact of the heating speed as well as of the value of J_{Cu} is similar to that found for the non-twisted conductor: in case of slow heating, the quench starts close to the end of the HFZ and the propagation is clearly faster in the case of high J_{Cu}, see the comparison between shot 161103 and 181101.

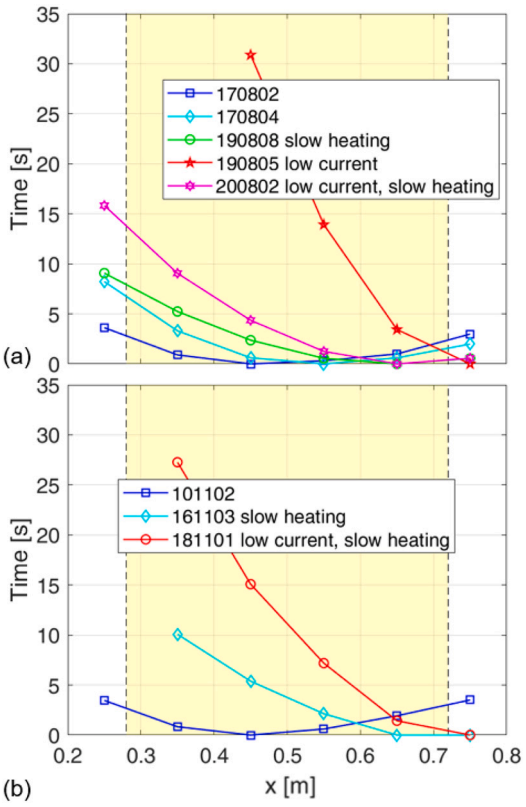

Fig. 3. Evolution of the quench front propagation for different shots on (a) non-twisted and (b) reference conductor. The high field zone (HFZ) is shown in yellow. The shot parameters are reported in Table 1.

Table 3
NZPV in mm/s in the non-twisted conductor.

Shot	VH1-V5	V5-V7	V7-V9	V9-VH3
170802	36.7	*	147.2	50.3
170803	23.3	51.5	*	68.2
170804	20.3	37.1	*	72.3
170805	30.3	*	135.7	46.1
170806	25.2	*	159.0	52.8
170808	21.1	42.5	*	51.9
190804	43.4	*	116.7	62.3
190808[a]	26.1	34.9	55.2	*
190805[b]	–	–	5.9	9.5
200802[c]	14.7	21.3	32.1	*

The asterisk is where the $E_{threshold}$ is reached first.
[a] Slow heating.
[b] Low J_{Cu}.
[c] Low J_{Cu}, slow heating.

A first direct comparison between the two conductors can be made on shot 190808 and shot 161103 on the non-twisted and reference conductor, respectively. These shots are chosen because they were performed with the same current, thus they have the same J_{Cu} and, being induced with a slow heating, they allow to compare in both cases the propagation of the upstream quench front. The selected shots show that the upstream quench front propagates more slowly in the case of the reference conductor. Comparing the front speed detected with the voltage taps at the same locations, i.e., V5-V7 with V6-V8 and V7-V9 with V8-V10, see Tables 3 and 4, the front propagates with a smaller speed in the reference conductor than in the non-twisted. This reduced velocity can be explained considering that the twisting allows having regions with a much higher critical current with respect to the non-twisted case. These regions with higher critical current should tend to slow down the quench propagation when the front gets close to them. On the other hand, in the non-twisted conductor this feature is not present and

Table 4
NZPV in mm/s in the reference conductor.

Shot	VH2-V6	V6-V8	V8-V10	V10-VH4
101102	38.0	*	75.5	63.2
101103	42.3	*	73.7	60.2
101104	36.4	*	72.2	60.6
161101	43.3	*	70.8	53.4
161102	38.2	*	74.0	54.5
161103[a]	N.A.	21.3	30.7	*
161104[a]	N.A.	21.0	30.7	*
161106[a]	N.A.	11.5	30.8	*
181101[b]	N.A.	8.20	12.6	*

The asterisk is where the $E_{threshold}$ is reached first.
[a] Slow heating.
[b] Low J_{Cu}, slow heating.

the quench does not encounter any major perturbation in the critical current distribution. Nevertheless, the two conductors exhibit different n-values, making less straightforward the direct comparison of the two conductors without the aim of a numerical model.

3.3. Virtual hotspot temperature

In contrast to the LTS conductors, the HTS conductors have a not negligible temperature gradient in the conductor cross-section, namely between jacket, helium and cable, as predicted in [25] and [17]. Consequently, in the experiment, not only (as usually done for LTS tests) the jacket temperature, but also the helium temperature is directly measured. Nevertheless, the hotspot cable temperature (namely, the copper and HTS stack temperature) is not measured. An experimental indication (the so-called "virtual sensor") of the hotspot temperature in the cable ($T_{hotspot}$), can be extracted from the voltage measurement ΔV_{ab} between two generic voltage taps a and b, following a well-established strategy for the LTS, see e.g. [26], solving for $T_{ab} = T_{hotspot}$ the implicit Equation (3),

$$\Delta V_{ab} = \rho_{Cu}(T_{ab}) \frac{L_{ab}}{A_{Cu}} \cdot I_{Cu} \tag{3}$$

where L_{ab} is the strand length between a and b, assuming that, from a simple electrical model with two resistors in parallel (jacket and Cu), it is possible to estimate the current I_{Cu} flowing at any time in the Cu (of the strands and of the Cu fraction of the HTS stacks), and assuming the dependence of the Cu (and steel) resistivity ρ_{Cu} on the temperature (and magnetic field) is known [27]. Note that the Cu resistivity also depends on the residual resistivity ratio (RRR) assumed here to be 100.

This procedure is based on the assumption that: 1. the cable temperature is uniform (both on the cross section and along the axis length) between a and b, i.e., $T(x) = T_{ab}$; 2. the entire length L_{ab} is normal, i.e. both quench fronts have already crossed both a and b. In order to compute the current repartition between cable, i.e. Cu, and jacket, it is also necessary to assume that the jacket and cable have the same temperature; although it is not strictly applicable, the effect of this assumption on the current repartition is small, because the steel resistivity relative variation with temperature is much smaller, in the considered range, than that of the Cu. While the second assumption can be guaranteed by the measurements, checking that the ΔV signals close to ΔV_{ab} measure non-zero voltage, the first assumption needs to be confirmed by a reliable numerical analysis.

In order to assess the validity of this method to estimate the $T_{hotspot}$, the H4C simulation results reported in Section 5 are used as reference, thanks to the good agreement between experimental and computed results (as far as the jacket and helium temperature is concerned), after the proper calibration of the code (see Section 4.3). Applying the above-mentioned methodology to the simulation results for the shot 170802, with special reference to the V5-V7 pair of voltage taps, the $T_{hotspot}$ estimated is ~140 K (with 0.5 kA in the jacket, 14.5 kA in the Cu).

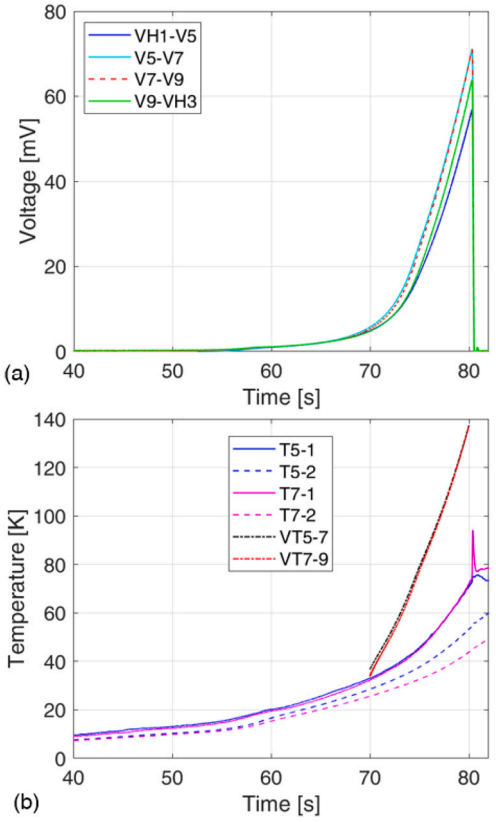

Fig. 4. Evolution of (a) the measured voltage and (b) of the measured temperature in the region within VH1 and VH3, for the shot 170802 (non-twisted conductor, 15 kA, 6 T, fast heating mode). In (b) the virtual hotspot temperature (VT) evaluated from a subset of the voltage measurements in (a) is also reported.

The evolution of the measured voltage and temperature in between VH1 and VH3 for shot 170802 is shown in Fig. 4. The $T_{hotspot}$ evaluated with the virtual temperature sensor shown in Fig. 4(b) is ~ 50-60 K higher than the measured helium temperature at t = 80 s, i.e., before the current dump. This comes from the comparison of the virtual temperatures VT5-7 and VT7-9 with the measured helium temperatures T5-1 and T7-1. Note that the local peak in T7-1 at t = 80 s is due to a response of the diagnostics to the current dump, rather than an actual fast increase in the helium temperature. The hotspot temperature in the cable looks then to be higher than the helium temperature, as expected. The $T_{hotspot}$ evaluation is further cross-checked with the H4C simulations, see Section 5.5.

4. Numerical model

The H4C code [20] simulates an arbitrary number of thermal, fluid and electric one-dimensional (1D) regions, solving the heat diffusion, a set of Euler-like equations and a diffusion-like equation, respectively. The dimension on which all the equations are solved is *along* the conductor axis, therefore the heat transfer between solid regions, e.g., the strands and the jacket, or between solid and fluid regions, e.g., the helium and the jacket, need to be lumped in a thermal contact resistance or a heat transfer coefficient, respectively. Especially the first quantity, i.e., the thermal contact resistance at the interface between solids, is hard to predict or measure, therefore it is calibrated on selected experimental shots of the conductor at hand. Note that the approach in the modeling of these conductors, i.e., 1D along the conductor axis as well as the need of calibration of free parameters is similar to that already employed with success for LTS conductors, see e.g., [23].

Table 5
Interface parameters and constitutive laws.

Thermal contact resistance	[m^2 K/W]
Stack-Copper	$8{\cdot}10^{-5}$
Copper-Copper	$5{\cdot}10^{-3}$
Copper-Stainless steel	$1{\cdot}10^{-4}$ (to be calibrated)
Friction factor correlation	Petukhov [28]
Nusselt number correlation	Dittus-Boelter [29] (to be calibrated)

To account in perspective for asymmetries due to, e.g., defects localized on a single strand, the 3 strands have been modeled separately.

The lumping strategies of the cross-section of the conductor sub-elements have been performed as follows: each strand is modeled with two thermal and electric regions (HTS stack and Cu profile around it). Together with a thermal and electric region for the jacket, the total number of electric and thermal regions is 7. On the other hand, the fluid is modeled with one single region.

The interface parameters between the different regions as well as the constitutive laws for the fluid and for the superconductor are reported in Table 5 and are taken from [25], if not otherwise stated. All the solid thermophysical properties implemented in the model for the solids are temperature dependent and, in case of the copper resistivity and thermal conductivity, also the magnetic field dependence is taken into account, implementing the properties reported in [27].

4.1. Boundary conditions

The boundary conditions considered in these preliminary simulations are the following (the computational domain goes from the inlet to the outlet of the conductor, i.e., from after the bottom joint until before the top joint, as shown in Fig. 1):

- Fluid model:
  - Inlet temperature: the experimental T1-1. This quantity is also used as reference for the synchronization between experimental and computed results.
  - Inlet and outlet pressure: such that the mass flow rate agrees with the measured one.
- Thermal model:
  - Fixed temperature (equal to T1-1) at the inlet end.
  - Zero heat flux (adiabatic) at the outlet ends.
- Current model:
  - Imposed current in the stacks at conductor outlet.
  - Zero current gradient, i.e., null voltage, imposed at conductor inlet.

4.2. Stack and cable twisting

The effect of the twisting on the critical current is taken into account using the approach proposed in [17]. The resulting twist-pitch has been computed as superposition of the two twist stages, leading to a twist pitch equal to 285 mm. The resulting distribution of critical current in the HFZ is shown in Fig. 5.

4.3. Model calibration

The rationale of the model calibration is to find the optimal value of free model parameters, i.e., the values that lead to the best agreement between computed and experimental results on a selected shot. In order to assess the soundness of such calibration, the same type of transient is simulated keeping frozen the model parameter on another – independent with respect to the previous – shot.

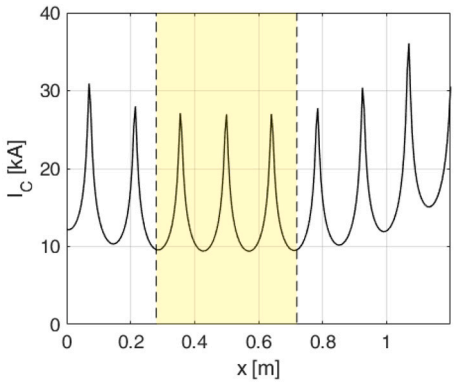

Fig. 5. Distribution of I_C in the first half of the reference conductor at 9 T and 5.7 K. The high field zone (HFZ) is shown in yellow.

4.3.1. Heat transfer coefficient

One of the free model parameters is the heat transfer coefficient between helium and Cu strand and between helium and jacket. It is a free parameter since it is still not measured on this geometry and/or it would require a dedicated analyzes, such as Computational Fluid Dynamics.

Thus, the rationale here is to find the best multiplier (M) to the Dittus-Boelter correlation based on the heat slug tests, i.e. tests where the fast heating was not strong enough to induce a quench.

The parametric study has been performed on one of the fast heating of shot 170802, see Fig. 6. The optimal value of M is between 0.05 and 0.1 and it is confirmed on a stronger fast heating (of the same shot), simulated with M = 0.06 and shown in Fig. 6(b). It is worth noticing that the helium and jacket temperature increases are well captured in the HFZ. However, the comparison with the T11-1 sensor (not shown) is not as satisfactory, especially for the helium temperature increase. Nevertheless, the most interesting region is the HFZ, therefore this (calibrated) model is then reliably used for the quench simulations.

4.3.2. Thermal contact resistance between strand and jacket

The other free model parameter is the thermal contact resistance between strand and jacket, i.e. between copper and stainless steel. The calibration of the thermal contact resistance (R_{th}) between the strand and the jacket, thus between copper and stainless-steel (Cu-SS), has been observed to play a major role on the quench propagation, in terms of speed of the voltage rise, and, in turn, of temperature rise.

It can be observed in Fig. 7 how a ~20% variation of the $R_{th,Cu-SS}$ affects the total voltage rise. The heat transfer coefficient corresponding to the $R_{th,Cu-SS}$ investigated here spans from 4000 to 7000 W/m^2/K.

The impact of R_{th} on the quench propagation is clear: the larger the R_{th}, the faster the voltage rise, because the heat capacity of the jacket is "less available" to the quenched region, which remains confined into the strands, therefore the temperature and voltage rise is faster.

The calibrated $R_{th,Cu-SS}$ agrees with the order of magnitude measured in [30]. Nevertheless, in [30], a strong temperature dependence of R_{th} from cryogenic to room temperature is found. Therefore, the constant value found in the calibration should be interpreted as an average value which is suitable over the temperature range span during the quench, i.e. 5 to 200 K. The impact of a temperature dependent R_{th} will be investigated in future work, because also the contribution due to the contact pressure is currently not known and in [30] was not measured.

5. Numerical results and comparison with the measurements

5.1. Non-twisted conductor, high J_{Cu}, fast heating

The soundness of the calibration of R_{th}, performed on shot 170802 has been cross-checked on another shot with the same magnetic field and current and with the quench triggered by fast heating, but with a

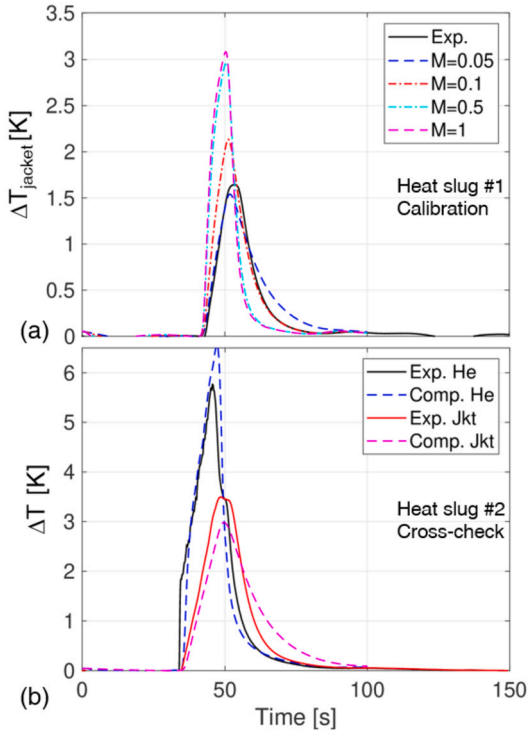

Fig. 6. (a) Calibration of the multiplier (M) on the increase of temperature $\Delta T(t) = T5(t) - T_0$ in the jacket at T5 with respect to the average temperature over 20 s before the slug T_0. (b) Cross-check of the calibration on a different slug.

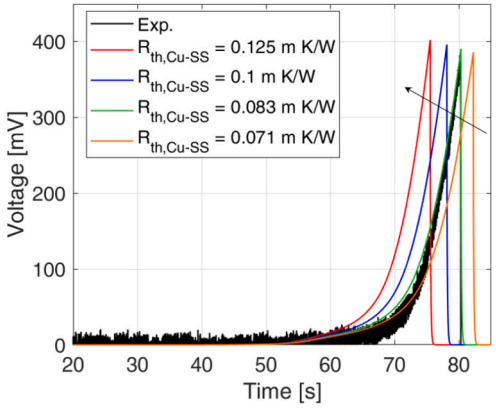

Fig. 7. Comparison of the experimental (Exp.) and computed total voltage evolution. The latter is shown as a function of the $R_{th,Cu-SS}$ (shot 170802 non-twisted conductor, 15 kA, 6 T, fast heating mode). The arrow shows the direction of increase of R_{th}.

higher dump temperature (shot 170808), thus with a longer evolution of the quench.

In the simulation of 170808, all the calibrated parameters are kept frozen. However, a degradation of the critical current has been found after the quench tests. In the case of the non-twisted conductor, a 3.2% degradation has been found, thus it has been supposed to go from 0% to 3.2% linearly after each quench test. Therefore, in the simulation of 170808, a 1% degradation of J_C was considered.

The comparison of the measured and computed total voltage and hotspot temperature evolution is reported in Fig. 8, showing a good agreement over the entire transient. The computed hotspot agrees within 8 K with that reconstructed from the experiment, which is a very good agreement, since it corresponds to a 3% relative error, computed

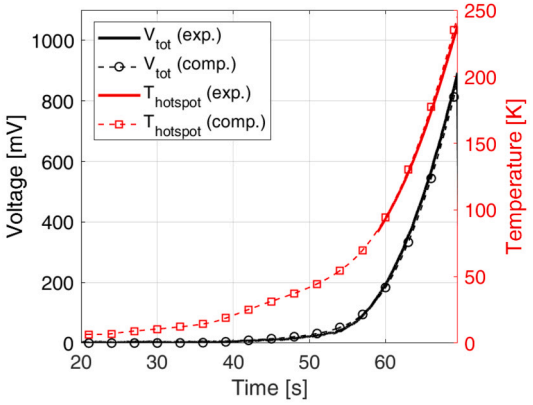

Fig. 8. Evolution of the measured (exp.) and computed (comp.) total voltage (V_{tot}) and hotspot temperature ($T_{hotspot}$) in shot 170808, non-twisted conductor.

as $err_{rel} = \left|\frac{T_{exp}-T_{comp}}{T_{exp}-T_0}\right|$, where T_{exp} and T_{comp} are the measured and computed maximum temperatures, respectively, and T_0 is the temperature before the helium starts being heated. The error is computed when the hotspot temperature (and the voltage) are at their maximum, in order to have a quantification of the error when the difference is the largest as well as when the most interesting quantities are computed, e.g., the maximum hotspot temperature. Note that the "measured" hotspot temperature is reconstructed from the local voltage measurement and the current repartition between the copper of the strands and the jacket, as described in Section 3.3. Furthermore, being the voltage taps very close, the virtual temperature is expected to be very close to the actual maximum temperature in the conductor, making the computed results even more reliable. This expectation is discussed (and confirmed) in Section 5.5, thanks to the computed temperature profiles.

The comparison of the local voltages and temperature is reported in Fig. 9. Also locally, the simulated results are in good agreement with the measured ones: the relative error on the voltage (where the maximum voltage is reached) is equal to 12% (computed as $err_{rel} = \left|\frac{V_{exp}-V_{comp}}{V_{exp}}\right|$, where V_{exp} and V_{comp} are the measured and computed maximum voltages, respectively), while the relative error on the helium and jacket temperature (where the maximum values are reached) are equal to 10% and 17%, respectively.

Note that the voltages are higher between taps V7-V9 and V9-VH3, meaning that the quench has started propagating on the downstream portion of the high field region. This is confirmed by the helium temperature sensors: the highest temperature is measured by T7 rather than T5, however it is expected to observe a shift downstream of the maximum helium temperature with respect to that of the solids because of the helium flow, see Section 5.5. Also the maximum jacket temperature is measured in T7, see Fig. 9. The measured and computed temperatures in T3 have a worse agreement with respect to the other (not shown). This could be due to the close proximity of T3 to the conductor inlet, thus it is expected to be very sensitive to the boundary conditions. Nevertheless, the quench never starts close to T3, thus the agreement on this temperature sensor is considered less important then that of the others.

5.2. Non-twisted conductor, low J_{Cu}

The other type of quench test analyzed on the non-twisted conductor is at higher field and lower current, thus low J_{Cu}, with respect to those adopted in the previous tests analyzed. Here, in shot 200802 the high field zone reaches 10 T and the current is kept at 11 kA (J_{Cu} = 73 A/mm^2), see Table 1. For comparison, the test analyzed in the previous section was performed at 6 T and 15 kA (J_{Cu} = 100 A/mm^2).

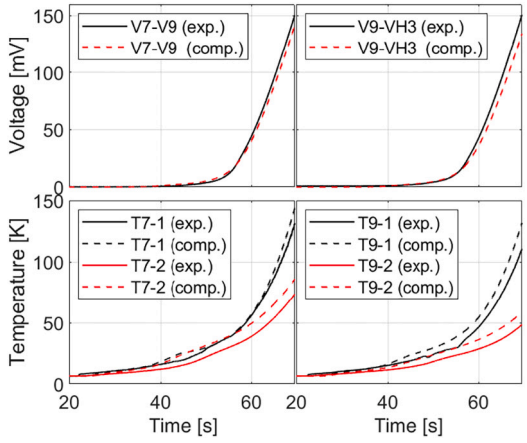

Fig. 9. Evolution of the measured (exp.) and computed (comp.) local voltage between taps V7-V9 and V9-VH3, helium (T7-1 and T9-1) and jacket (T7-2 and T9-2) temperature in shot 170808, non-twisted conductor.

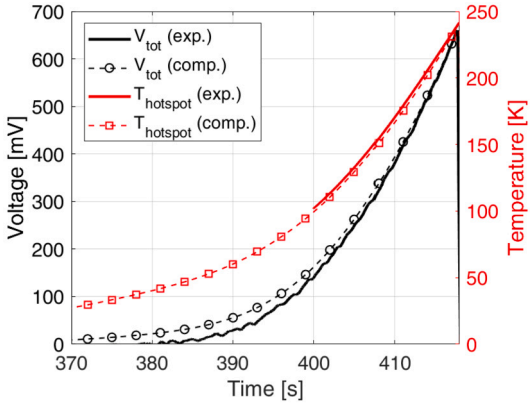

Fig. 10. Evolution of the measured (exp.) and computed (comp.) total voltage (V_{tot}) and hotspot temperature ($T_{hotspot}$) in shot 200802, non-twisted conductor.

Coherently with the procedure described before, here the J_C degradation is assumed to be equal to 3%.

The comparison between measured and computed results is shown in Fig. 10. In this case, the agreement is even better than before, meaning also that the scaling law adopted is well suited. The maximum difference in the hotspot is 2-3 K, i.e., $err_{rel} = 1\%$.

The local voltages and temperature are compared in Fig. 11. It can be observed that the quenched region is shifted on the downstream side of the high field region, even more than the case at low J_{Cu}, since the voltage between V9-VH3 is (slightly) higher than V7-V9, which is in turn higher than V5-V7. The reason behind this is discussed in Section 5.5. Also in this case, the overall agreement is very good ($err_{rel} = 4\%$ where the maximum local voltage is reached), except for the first sensors (VH1-V5 and T3-2), in which the computed results are slightly higher than the measured ones (in this shot the T5-1 sensor was not working).

The computed helium temperature in T7 is few tens of K higher than the measured one; however the hotspot temperature agrees very well with that reconstructed from the experiment. This hints that the code is computing the correct values of temperature, but slightly shifted in position with respect to the experiment. Therefore, comparing the computed and measured values at the same locations lead to few tens of K of difference, but comparing the absolute values, such as the hotspot temperature, a better agreement is found. This point is discussed further in Section 5.5. Nevertheless, the relative error where and when the maximum helium and jacket temperatures are reached, i.e. on T9, is small and it is equal to 13% and 10%, respectively.

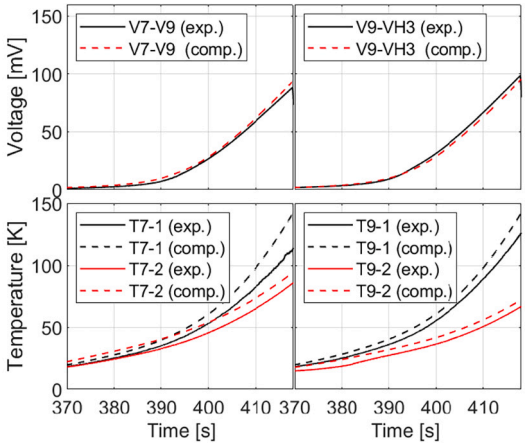

Fig. 11. Evolution of the measured (exp.) and computed (comp.) local voltage between taps V7-V9 and V9-VH3, helium (T7-1 and T9-1) and jacket (T7-2 and T9-2) temperature in shot 200802, non-twisted conductor.

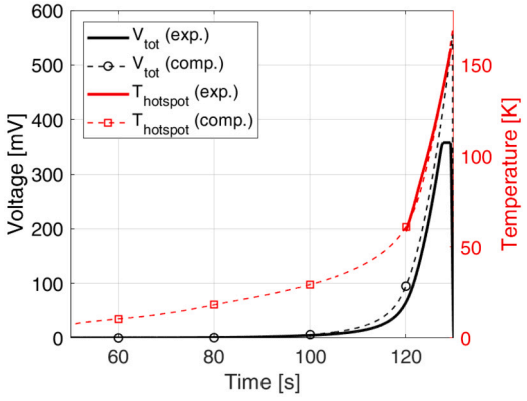

Fig. 12. Evolution of the measured (exp.) and computed (comp.) total voltage (V_{tot}) and hotspot temperature ($T_{hotspot}$) in shot 101102, reference conductor.

5.3. Reference conductor, high J_{Cu}

The results of the simulation of the shot 101102 (low field, 3.5 T, high current, 15 kA, thus high $J_{Cu} = 100\ A/mm^2$) on the reference conductor are presented here. In these simulations, the same parameters calibrated for the non-twisted conductor have been kept, even though is not necessary that they should be the (exactly) the same. For example, the $R_{th,Cu-SS}$ is a function of the applied pressure at the materials interface and it can be slightly different since the conductors are manufactured "manually". Most likely, the $R_{th,Cu-SS}$ is weakly dependent on the pressure at the interface, thus the reference conductor does not require a new calibration on $R_{th,Cu-SS}$.

The computed total voltage and hotspot temperature agree well with the measured ones, see Fig. 12. The hotspot temperature differs by only 3 K (~ 2%). Note that the total voltage signal is different with respect to that used in the non-twisted conductor and it saturates at 370 mV.

Computed and measured local quantities in the HFZ are reported in Fig. 13. Except for an overestimation of the voltage close to the inlet, the agreement is good, in particular in the most relevant region, which is around sensors T6 and V6-V8, i.e., where the maximum voltages and temperatures are reached, with a relative error on the voltage, helium and jacket temperature equal to 17%, 10% and 28%, respectively. Note that, in this case, the quench starts very close to the magnetic center.

5.4. Reference conductor, low J_{Cu}

The measured and computed results of a shot at high field (9 T) and low current (9.5 kA, $J_{Cu} = 63\ A/mm^2$), shot 181101, is presented in

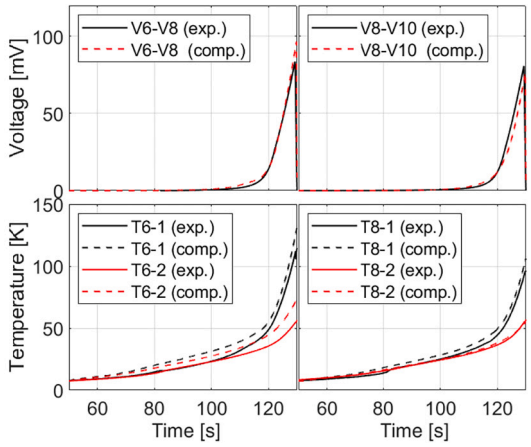

Fig. 13. Evolution of the measured (exp.) and computed (comp.) local voltage between taps V6-V8 and V8-V10, (b) helium (T6-1 and T8-1) and jacket (T6-2 and T8-2) temperature in shot 101102, the reference conductor.

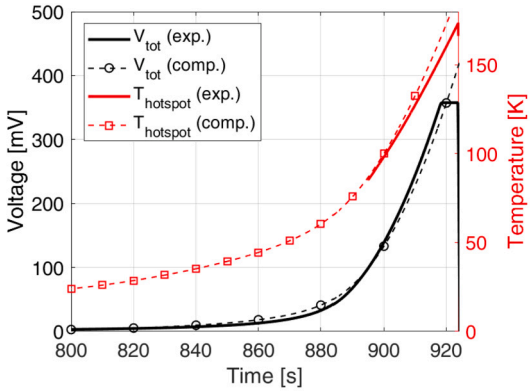

Fig. 14. Evolution of the measured (exp.) and computed (comp.) total voltage (V_{tot}) and hotspot temperature ($T_{hotspot}$)in shot 181101, reference conductor.

this section. In these simulations, the degradation of J_C is supposed to be equal to 3%, according to the rationale adopted also for the non-twisted conductor.

The total voltage and hotspot temperature are reported in Fig. 14. Also in this case, the agreement between measured and computed results is good. The maximum difference between measured and computed hotspot temperature within 15 K (~12%).

It is worth noting that the voltage rise in case of high field, low current is much slower than the case at low field, high current: in the high current case, it takes 10 s to go from 50 mV to 400 mV, while in the low current case it takes 40 s. The discussion on this topic is done in Section 5.5.

The comparison of the computed and measured local quantities is shown in Fig. 15. Also in this case the agreement is good and the different behavior of the quench evolution, i.e., shifted in the downstream portion of the high field region, is well reproduced by the model. Again, in this case, the voltage in the region close to the inlet is slightly overestimated, but still the region where the maximum voltage is reached, i.e., where the highest temperature is reached, is well reproduced (relative error on local voltage, helium and jacket temperature equal to 8%, 10% and 1%, respectively).

5.5. Quench front propagation and temperature profiles

The comparison between the computed and measured quench front propagation is discussed here, for both non-twisted and reference conductors. The position of the front in the experiment is reconstructed with the same rationale already adopted in Section 3.2.1, i.e., the front

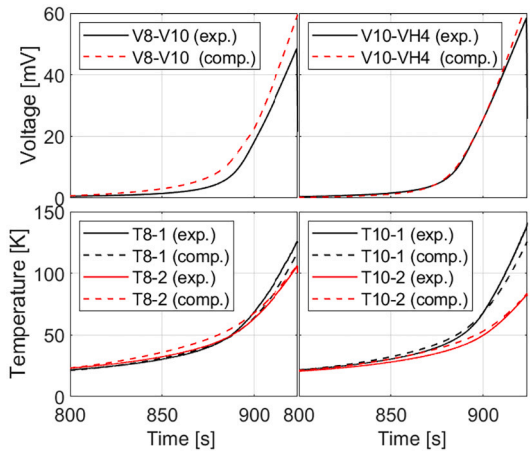

Fig. 15. Evolution of the measured (exp.) and computed (comp.) local voltage between taps V8-V10 and V10-VH4, helium (T8-1 and T10-1) and jacket (T8-2 and T10-2) temperature in shot 181101, reference conductor.

is assumed to be between two voltage taps when 10 mV are measured. Recalling that the distance between the voltage taps in the HFZ is 10 cm, this criterion is equivalent to having an average electric field of 1 mV/cm. Since an average criterion is considered, the position of the quench front is represented as an interval 10 cm wide at the time at which the criterion is reached, see the green areas in Figs. 16 and 17.

The computed position of the quench front is tracked when the *local* electric field reaches 1 mV/cm. Regarding the non-twisted conductor, the comparison of the computed and measured quench front propagation is in good agreement for both the high and low J_{Cu}, both in terms of position of the quench initiation and in terms of propagation. This implies also the propagation speed is well captured by the model. Indeed, it is confirmed that, in case of high J_{Cu}, the quench starts close to the magnetic center, see Fig. 16(a), while in case of low J_{Cu} it starts close to the downstream edge of the HFZ, see Fig. 16(b).

The numerical tool has been also used to extract the information on where and how the current sharing starts, i.e., tracking the position at which $I = I_C$. In the case of low J_{Cu} the first point where $I = I_C$ is at the magnetic center, $x = 0.5$ m, as in the case at high J_{Cu}, but the point at which the quench propagation actually starts is moved several cm downstream ($x = 0.6$ m, see Fig. 16(b)) as a consequence of the slow heating as well as of the less strong propagation, due to the lower J_{Cu}. It is worth noting that the time when for the first time $I = I_C$ ($t = 22$ s in shot 170808, $t = 142$ s in shot 200802), i.e., an electric field of 1 μV/cm, and the time at which for the first time 1 mV/cm is reached ($t = 53$ s in shot 170808, $t = 390$ s in shot 200802) are very different, i.e., the quench takes a long time to actually start propagating, if compared to LTS conductors, see [23]. In HTS conductors it takes few to several tens of seconds to go from 1 μV/cm to 1 mV/cm, while in LTS conductors it was found to happen on time scales smaller than 1 s. This could be explained comparing the dependence of J_C on the temperature: in case of typical LTS, J_C decreases very fast in case of a temperature increase, while in HTS the J_C is flatter with respect to the temperature.

Concerning the quench front propagation in the reference conductor, as illustrated in the Fig. 17, the impact of the twisting is clear on the evolution of the normal zone. Regions where the J_C is higher (not shown in the figure) are the last where the electric field rises, while in the low J_C regions, the electric field rises before. In both cases, i.e., high and low J_{Cu}, the computed quench front propagation intersects the available measured intervals. Note that the measurements tend to smooth the actual shape induced by the J_C distribution. Nevertheless, the overall behavior is reproduced by the computed results. Also on this kind of conductor, the electric field takes several tens of seconds to go from 1 μV/cm to 1 mV/cm.

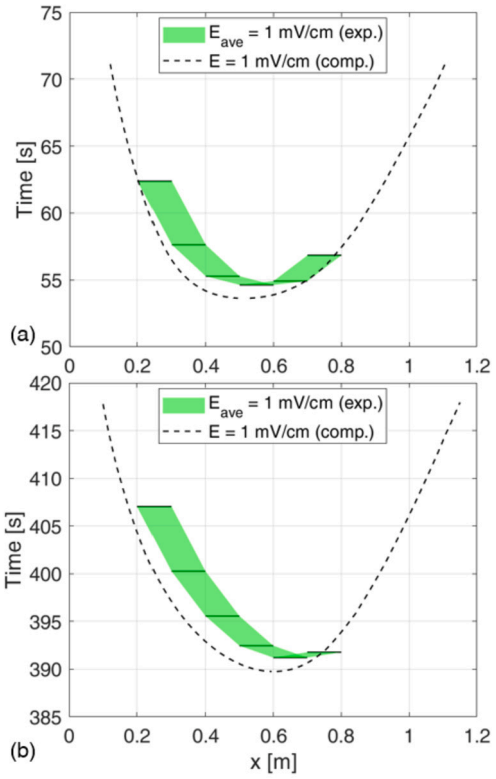

Fig. 16. Computed (dashed lines) and measured (green shaded areas) quench front propagation in the non-twisted conductor in shot (a) 170808 and (b) 200802. E = 1 mV/cm is the electric field chosen for both the experimental data (exp.) and the computed results (comp.)

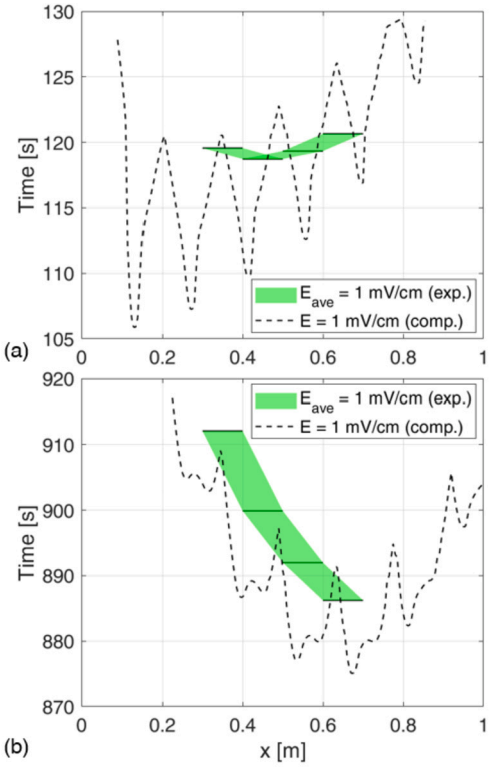

Fig. 17. Computed (dashed lines) and measured (green shaded areas) quench front propagation in the reference conductor in shot (a) 101102 and (b) 181101. E = 1 mV/cm is the electric field chosen for both the experimental data (exp.) and the computed results (comp.)

The temperature profiles obtained with the simulations, having assessed the accuracy of the model in the previous sections, can now be reliably analyzed. The profiles are extracted from the simulations at the same total voltage (640 mV, i.e., close to the maximum voltage reached in case of low J_{Cu}) on the non-twisted conductor.

The quench at high J_{Cu} leads to a hotspot located close to the center of the HFZ, while in case of low J_{Cu} it is moved towards the downstream end of the HFZ, see Fig. 18. This is a consequence of the previous discussion on the NZPV: in case of high J_{Cu}, the quench propagation is faster, thus the helium is prevented from advecting downstream the normal zone. On the other hand, in case of low J_{Cu}, the NZPV is lower, therefore the helium can be heated more slowly than the case at high J_{Cu} in the region in current sharing, pushing downstream the normal zone. Coherently, the largest hotspot temperature is reached in the case of lower NZPV, since the normal zone propagates at a lower speed, thus, looking at the same total voltage, the resistance (and, in turn, the temperature) must be higher to get the same voltage at lower current. Note that the strand temperature, where the maximum temperature is reached, varies by a few K over 10 cm. Therefore, the virtual temperature reconstructed from the voltage where the latter is the largest is very close to the actual maximum temperature, as mentioned in Section 5.2.

From Fig. 18, it can be seen that the jacket temperature reflects the shape of the strand temperature, thus the region at high temperature in the jacket (which is also measured) is also the high temperature region of the strands. On the other hand, it is shown that the helium advection is clear and the helium temperature profile is shifted downstream by 20 cm in both cases.

It is also shown that the computed results match the experimental measurements taken at the same time. In particular, in both cases the macroscopic differences are very well reproduced, i.e., wider high temperature region and larger hotspot in case of low J_{Cu} as well as helium temperature profile moved towards the outlet with respect to the strand and jacket temperatures. Also, the strand temperature is reproduced within the bands which delimit the interval over which the virtual temperature is computed, i.e. the distance between adjacent voltage taps, confirming the reliability of the model in assessing crucial quantities such as the hotspot temperature as well as key behavior in such conductors, e.g., the helium advection.

6. Impact of the magnetic field profile and quench initiation strategy

In this section, the impact on the quench propagation of different magnetic field profiles and initiation strategies is discussed. The interest comes from the need to assess how much a quench test in SULTAN is representative of a quench in a real conductor configuration. The operating condition of these conductors, i.e., that foreseen in the EU DEMO CS, is well approximated with a uniform magnetic field profile. Therefore, here we compare the results of quench simulations obtained with a uniform magnetic field against those coming from simulations with a SULTAN-like magnetic field distribution, i.e., with a short region at ~uniform (maximum) magnetic field. The conductor examined here is the not-twisted sample. The same model, operating and boundary conditions discussed for the shot 170808 are used. The only difference is the magnetic field distribution. Note, however, that another relevant difference between the operating conditions expected in the CS and those tested in SULTAN is the margin. Indeed, in order to initiate the quench by warming the helium, it was needed to have a ratio I/I_C close to 95%, while in the CS a ratio of I/I_C closer to 80% is expected. The analysis of the quench on a conductor in the operating conditions of the EU DEMO CS is performed in Section 7. Here, the impact of the magnetic field profile only is analyzed.

It can be seen in Fig. 19(a) that the hotspot temperature grows much more in the case of a SULTAN-like magnetic field distribution, for the same total voltage. This is due to the much slower propagation induced by the peaked shape of the SULTAN field and can be observed in the

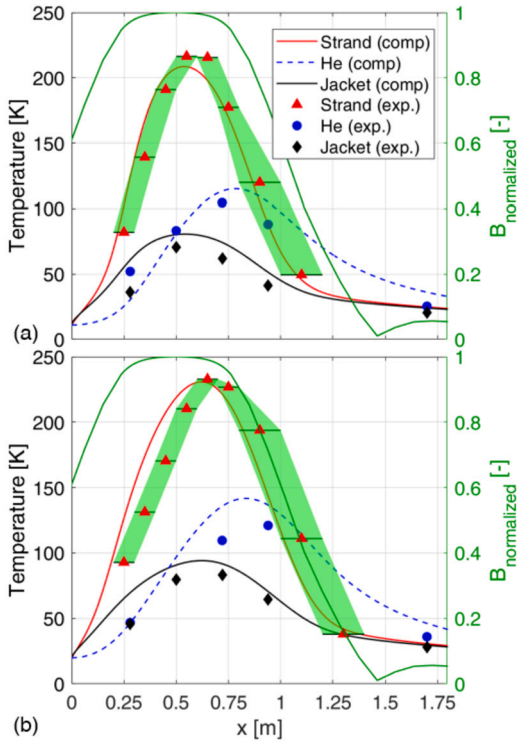

Fig. 18. Computed (comp, in the legend) strand, jacket and helium (He) temperature profiles in the first 1.8 m of the non-twisted conductor in case of (a) high J_{Cu} and (b) low J_{Cu} at the max total voltage of 640 mV. The measured (exp.) temperatures of strand, jacket and helium (He) are reported as symbols. The measured strand temperatures are reconstructed from the voltage measurements over 10 cm or 20 cm. The interval covered by each voltage tap pair is highlighted in green. The symbols for the strand temperature are placed in the midpoint of the voltage taps. The magnetic field profile is also shown in green.

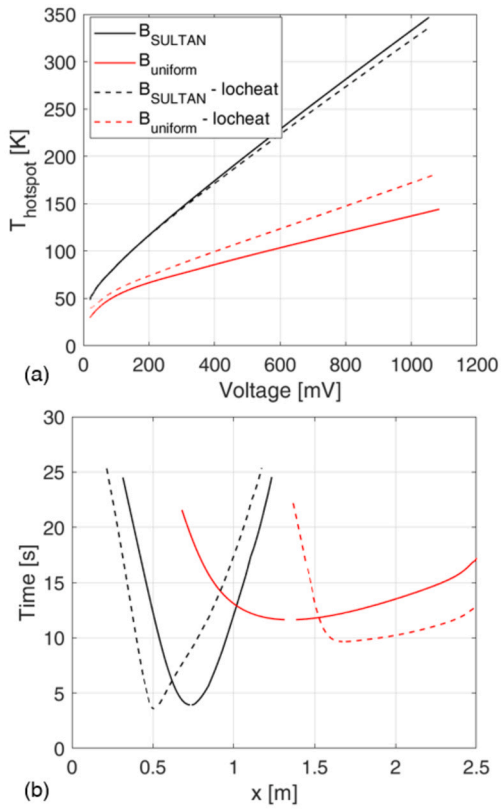

Fig. 19. (a) Hotspot temperature as function of the total voltage and (b) quench front propagation for different magnetic field profiles (either uniform ($B_{uniform}$) or that corresponding to the SULTAN one (B_{SULTAN}), reported in Fig. 1) and quench initiation strategies (either warm He ingress in the conductor or with localized external heat deposition, *locheat* in the legend).

quench front propagation shown in Fig. 19(b). In case of uniform magnetic field distribution, the quench propagates faster, thus leading to a smaller hotspot temperature, when the same total voltage is considered. This is caused, in turn, by the larger temperature margin seen by the quench front as it "hits" the decreasing magnetic field in case of the SULTAN-like distribution. Furthermore, in case of uniform field, the role of the helium moving the downstream front at a higher speed than the upstream front can be appreciated more.

With the same two models, a different quench initiation strategy has been tested, i.e., a 5 cm localized heating for 200 ms, with a constant inlet temperature, rather than a warm helium entering the conductor. This test was motivated by the observation that the SULTAN field is actually uniform for 44 cm, thus we wanted to analyze whether a quench initiated locally at the center of the region where the SULTAN field is uniform would have given results closer to the uniform field case. It can be seen in Fig. 19(a) and (b) that the two simulation with the same SULTAN field provides the very same results, independently on the quench initiation strategy. On the other hand, the quench induced with a localized heating in the uniform field case propagates slightly slower than that induced warming the helium flow. This is due to the pre-heating of the cable after the warm helium has passed, thus reducing the margin to quench, which indeed propagates faster; this is clear looking at the upstream front in the two uniform field cases in Fig. 19(b). This in turn leads to slightly lower hotspot temperatures in case of quench induced with warm helium, see again Fig. 19(a).

These analyzes show that the impact of the shape of the field present in SULTAN is evident on the results of interest, e.g., the hotspot temperature and quench front propagation. Nevertheless, the tests in SULTAN have allowed having

- a measure of the relevant quantities in high field, high current conductors, which has been shown to be clearly conservative with respect to the uniform field case.
- a rich database over which thermal-hydraulic codes can be calibrated and validated and can then be used with the acquired reliability to simulate real-case scenarios. The alternative would be to test a long length conductor, e.g., in the bore of the CSMC in Naka as done for the ITER CS [26] and TF [23] Insert Coils, at a much higher cost. This cannot be afforded for multiple conductor designs as the Quench Experiment campaign in SULTAN allows.
- the possibility to test several conductors to investigate the impact of different feature in the design on quench propagation, allowing in turn to shorten the list of possible candidates to the design and manufacturing of a potential Insert Coil.
- showing that a non-negligible degradation is present as a consequence of quench tests on which further investigation is needed to reach a more robust and resilient design.

Therefore these analyzes confirm the relevance of the results obtained in the upgraded SULTAN facility in the Quench Experiment campaign.

7. Preliminary quench simulation in DEMO-relevant conditions

A recent study on the quench propagation in an HTS conductor currently proposed for the EU DEMO hybrid CS option was performed in [31]. The numerical model adopted in that work has been modified in order to take into account the information coming from the work presented here, e.g., the calibrated parameters for the helium heat transfer coefficient and the thermal contact resistance between copper and stainless steel.

Table 6
Operating conditions and geometrical parameters of the conductor analyzed.

Parameter	Value
T_{op} [K]	4.5
$I_C(T_{op}, B_{max})$ [kA]	59.7
$T_{CS}(J_{op}, B_{max})$ [K]	12.7
Hydraulic length [m]	739
A_{Cu} [mm^2]	480
A_{SC} [mm^2]	1.7
A_{SS} [mm^2]	4550
A_{He} [mm^2]	139

The quench is initiated when the current and magnetic field are the largest (46.25 kA and 15 T, respectively), i.e., at the end of the coil charge (lasting 500 s), depositing energy with a 100 ms long and 10 cm wide external heat deposition. The parameters of the full-scale conductor analyzed in DEMO-relevant conditions are reported in Table 6. It features six twisted stack strand enclosed in a copper profile (as the three strands of the sub-sized cable tested in SULTAN and analyzed here), twisted around a central copper core, see Figure 2 in [31].

The setup of the simulation is the same described in [31], e.g., only coupling losses are taken into account in case of magnetic field variation since hysteresis losses are currently being quantified. The voltage threshold considered is 0.3 V (a more conservative and realistic value with respect to the optimistic value targeted for the EU DEMO, i.e., 0.1 V [32]) with a delay time, i.e., time interval after the detection and before the start of the current discharge, equal to 1.1 s. The current discharge time constant is assumed equal to 15 s.

The most relevant result is reported in Fig. 20, showing that a hotspot temperature of roughly 250 K is reached in the superconductor in case a 0.3 V quench threshold is considered. This implies that the hotspot temperature reached adopting a conventional quench detection strategy could stay below the ITER criterion of having a maximum hotspot temperature in the cable bundle below 250 K (which is the same criterion currently adopted as reference in EUROfusion [32]). The voltage threshold is believed to be possibly improved (reduced), thus reducing the hotspot. Note, however, that 250 K is still an ITER reference value, thus a threshold suitable for HTS conductors should be considered as soon as it will be identified. Furthermore, this preliminary analysis does not include many details of the coil technology, such as joints, insulation etc., therefore further, more detailed analysis is needed to accurately extrapolate the quench behavior to the full coil. The result obtained here shows that a quench in such a conductor, even with a 0.3 V threshold (which is three times the threshold currently considered in EUROfusion for LTS magnets) does not lead to prohibitive hotspot temperature. This implies that a voltage-based quench detection system could still be considered as one of the possible candidates for quench detection in HTS coils.

It is worth highlighting that this is one of the first results concerning the analysis of real case scenario quench simulation carried out with a tool calibrated on large scale quench experiment.

8. Conclusions and lessons learnt

The analysis of the experimental data collected during the recent Quench Experiment campaign carried out at SULTAN on high current, high field sub-size HTS conductors was carried out, showing that a normal zone propagation velocity (NZPV) of tens of mm/s is reached with an hotspot temperature of 240 K, corresponding to a total voltage of more than 600 mV at a J_{Cu} value of 100 A/mm^2.

The comparison of the experimental results on twisted and non-twisted conductor has shown that a slightly higher NZPV is present in the non-twisted conductor.

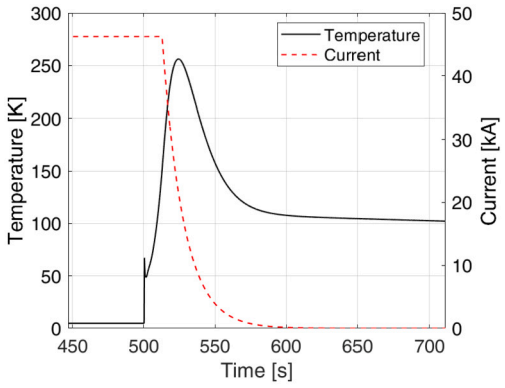

Fig. 20. Evolution of the hotspot temperature (black solid line and of the current (red dashed line in the full scale EU DEMO CS conductor (hybrid option, layer 1).

A thermal-hydraulic and electric model implemented in the H4C code has been developed, calibrated and applied to the analysis of the quench experiments, showing that the model is able to reproduce with a very good agreement both global, e.g., total voltage, and local quantities, e.g., local voltage and helium and jacket temperature.

The calibration process has shown the impact of parameters such as the thermal contact resistance between copper and stainless steel on the quench evolution. This confirms the relevance of the tests carried out, which allowed the calibration of numerical models, as well as the need for dedicated experiments to quantify or at least reduce the uncertainties on the (many) free parameters adopted in the numerical models typically adopted for such analyzes.

The validated model was then used to assess the impact of the quench initiation strategy as well as of the magnetic field distribution, showing that the heating strategy in SULTAN has no effects on the main quantities of interest, such as the hotspot temperature. However, the SULTAN magnetic field, being uniform for only few tens of cm, leads to higher hotspot temperature than in case of uniform magnetic field. Nevertheless, the quench experiments were fundamental to validate the numerical models. For future tests, a margin closer to that expected in operation should be used, in order to obtain results even more representative of a quench in the EU DEMO CS.

A preliminary projection to the EU DEMO CS full conductor quench, carried out with calibrated and validated H4C model, shows that, with a realistic quench detection threshold of 0.3 V, a hotspot temperature of about 250 K is reached, i.e., the ITER limit set for the maximum superconductor temperature to be reached during a quench, meaning that a conventional quench detection strategy based on voltage measurement could be a candidate for detecting the quench in HTS coils. On this point, further more detailed analysis is needed.

CRediT authorship contribution statement

A. Zappatore: Conceptualization, Formal analysis, Methodology, Software, Visualization, Writing – original draft. **R. Bonifetto:** Resources, Supervision, Writing – review & editing. **P. Bruzzone:** Conceptualization, Methodology, Resources, Supervision, Writing – review & editing. **V. Corato:** Funding acquisition, Project administration, Resources, Writing – review & editing. **O. Dicuonzo:** Data curation, Investigation, Methodology, Validation, Writing – review & editing. **M. Kumar:** Data curation, Investigation, Writing – review & editing. **K. Sedlak:** Conceptualization, Methodology, Writing – review & editing. **B. Stepanov:** Data curation, Investigation, Writing – review & editing.

Declaration of competing interest

The authors declare the following financial interests/personal relationships which may be considered as potential competing interests:

Andrea Zappatore reports financial support was provided by European Consortium for the Development of Fusion Energy.

Data availability

The data that has been used is confidential.

Acknowledgement

This work has been carried out within the framework of the EUROfusion Consortium, funded by the European Union via the Euratom Research and Training Programme (Grant Agreement No 101052200 – EUROfusion). Views and opinions expressed are however those of the author(s) only and do not necessarily reflect those of the European Union or the European Commission. Neither the European Union nor the European Commission can be held responsible for them.

References

[1] Corato V, Vorpahl C, Sedlak K, Anvar V, Bennet J, Biancolini M, et al. Fusion Eng Des 2022;174:112971. ISSN 0920-3796.
[2] Sarasola X, Wesche R, Ivashov I, Sedlak K, Uglietti D, Bruzzone P. IEEE Trans Appl Supercond 2020;30:4200705.
[3] Martovetsky N, Freudenberg K, Hatfield D, Rossano G, Reiersen W, Khumthong K, et al. Fusion Eng Des 2021;164:112169. ISSN 0920-3796.
[4] Murakami H, Tsuchiya K, Kawano K, Kizu K, Hamada K, Itashiki Y, et al. IEEE Trans Appl Supercond 2021;31:4201005.
[5] Sedlak K, Anvar VA, Bagrets N, Biancolini ME, Bonifetto R, Bonne F, et al. Supercond Sci Technol 2020;33:044013.
[6] Bruzzone P, Fietz WH, Minervini JV, Novikov M, Yanagi N, Zhai Y, Zheng J. Nucl Fusion 2018;58:103001. https://doi.org/10.1088/1741-4326/aad835.
[7] Mitchell N, Zheng J, Vorpahl C, Corato V, Sanabria C, Segal M, et al. Supercond Sci Technol 2021;34:103001.
[8] Celentano G, De Marzi G, Fabbri F, Muzzi L, Tomassetti G, Anemona A, Chiarelli S, Seri M, Bragagni A, Della Corte A. IEEE Trans Appl Supercond 2014;24:4601805.
[9] Uglietti D, Wesche R, Bruzzone P. IEEE Trans Appl Supercond 2014;24:4800704.
[10] Wolf MJ, Bayer CM, Fietz WH, Heller R, Schlachter SI, Weiss KP. IEEE Trans Appl Supercond 2016;26:4801504.
[11] Mulder T, Dudarev A, Mentink M, Silva H, Van Der Laan D, Dhalle M, et al. IEEE Trans Appl Supercond 2016;26:4803605.
[12] Hartwig ZS, Vieira RF, Sorbom BN, Badcock RA, Bajko M, Beck WK, et al. Supercond Sci Technol 2020;33:11LT01. https://doi.org/10.1088/1361-6668/abb8c0.
[13] Du J, Sun J, Nie Y, Mo S, Cai Y, Chen H, et al. CSEE J. Power Energy Syst. 2021;7:150–5.
[14] van Nugteren J, Dhallé M, Wessel S, Krooshoop E, Nijhuis A, ten Kate H. Phys Proc 2015;67:945–51. ISSN 1875-3892.
[15] Savoldi Richard L, Casella F, Fiori B, Zanino R. Cryogenics 2010;50:167–76. ISSN 0011-2275.
[16] Bottura L, Rosso C, Breschi M. Cryogenics 2000;40:617–26. ISSN 0011-2275.
[17] Kang R, Uglietti D, Wesche R, Sedlak K, Bruzzone P, Song Y. IEEE Trans Appl Supercond 2020;30:5700107.
[18] Zappatore A, Augieri A, Bonifetto R, Celentano G, Marchetti M, Vannozzi A, et al. IEEE Trans Appl Supercond 2021;31:4800805.
[19] Oberkampf WL, Roy CJ. Verification and validation in scientific computing. Cambridge University Press; 2010.
[20] Zappatore A, Heller R, Savoldi L, Wolf MJ, Zanino R. Supercond Sci Technol 2020;33:065004.
[21] Dicuonzo O, Kang R, Sedlak K, Stepanov B, Uglietti D, Wesche R, et al. IEEE Trans Appl Supercond 2021;31:9500505.
[22] Heller R, Gade PV, Fietz WH, Vogel T, Weiss KP. IEEE Trans Appl Supercond 2016;26:4201105.
[23] Zanino R, Bonifetto R, Brighenti A, Isono T, Ozeki H, Savoldi L. Supercond Sci Technol 2018;31:035004.
[24] Wilson E. Superconducting magnets. Oxford Science Publications; 1992.
[25] Zappatore A, Fietz WH, Heller R, Savoldi L, Wolf MJ, Zanino R. Supercond Sci Technol 2019;32:084004.
[26] Bonifetto R, Isono T, Martovetsky N, Savoldi L, Zanino R. IEEE Trans Appl Supercond 2017;27:4700308.
[27] Drexler ES, Reed RP, Simon NJ. Properties of copper and copper alloys at cryogenic temperatures. NIST monograph, vol. 177. Washington, DC: U.S. Government Printing Office; 1992.
[28] Petukhov BS, Irvine TF, Hartnett JP. Advances in heat transfer. Hoboken, NJ: Wiley; 2009.
[29] Bergman TL, Lavine AS, Incropera FP, Dewitt DP. Fundamentals of heat and mass transfer. New York: John Wiley & Sons; 2011.
[30] Wolf MJ, Heller R, Fietz WH, Weiss KP. Cryogenics 2019;104(102980). ISSN 0011-2275.
[31] Zappatore A, Bonifetto R, Sarasola X, Zanino R. IEEE Trans Appl Supercond 2022;32:4203809.
[32] Corato V. Common operating values for DEMO magnets design for 2016. https://scipub.euro-fusion.org/wp-content/uploads/eurofusion/WPMAGREP16_16565_submitted.pdf, 2016. [Accessed 30 November 2016].